Predictions of the interfacial free energy along the coexistence line from single-state calculations ⊘

Special Collection: 2024 JCP Emerging Investigators Special Collection

Ignacio Sanchez-Burgos ⓘ ; Pablo Montero de Hijes ⓘ ; Eduardo Sanz ⓘ ; Carlos Vega ⓘ ;
Jorge R. Espinosa ✉ ⓘ

Check for updates

View Online   Export Citation

Articles You May Be Interested In

Solid-liquid interface free energies of pure bcc metals and B2 phases

J. Chem. Phys. (April 2015)

Temperature dependence of the crystal-liquid interfacial free energy and the endpoint of the melting line

J. Chem. Phys. (December 2013)

Determination of the solid-liquid interfacial free energy along a coexistence line by Gibbs–Cahn integration

J. Chem. Phys. (September 2009)
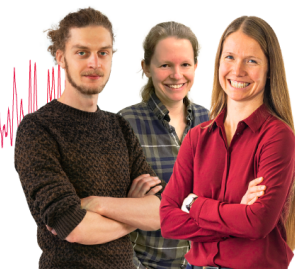
Predictions of the interfacial free energy along the coexistence line from single-state calculations

View Online   Export Citation   CrossMark

Ignacio Sanchez-Burgos,[1] (iD) Pablo Montero de Hijes,[2,3] (iD) Eduardo Sanz,[4] (iD) Carlos Vega,[4] (iD) and Jorge R. Espinosa[1,4,a)] (iD)

AFFILIATIONS

[1] Maxwell Centre, Cavendish Laboratory, Department of Physics, University of Cambridge, JJ Thomson Avenue, Cambridge CB3 0HE, United Kingdom
[2] Faculty of Physics, University of Vienna, 1090 Vienna, Austria
[3] Faculty of Earth Sciences, Geography and Astronomy, University of Vienna, 1090 Vienna, Austria
[4] Department of Physical-Chemistry, Universidad Complutense de Madrid, Av. Complutense s/n, 28040 Madrid, Spain

Note: This paper is part of the 2024 JCP Emerging Investigators Special Collection.
a)Author to whom correspondence should be addressed: jorgerene@ucm.es

ABSTRACT

The calculation of the interfacial free energy between two thermodynamic phases is crucial across various fields, including materials science, chemistry, and condensed matter physics. In this study, we apply an existing thermodynamic approach, the Gibbs–Cahn integration method, to determine the interfacial free energy under different coexistence conditions, relying on data from a single-state calculation at specified pressure and temperature. This approach developed by Laird *et al.* [J. Chem. Phys. **131**, 114110 (2009)] reduces the computational demand and enhances efficiency compared to methods that require separate measurements at each thermodynamic state. The integration scheme computes the excess interfacial free energy using unbiased constant volume, temperature, and number of particle simulations (NVT), where the two phases coexist, to provide input for the calculations. We apply this method to the Lennard-Jones and mW water models for liquid–solid interfaces, as well as the Lennard-Jones and TIP4P/2005 models for liquid–vapor interfaces. Our results demonstrate the accuracy and effectiveness of this integration route for estimating the interfacial free energy along a coexistence line.

I. INTRODUCTION

The study of interfaces between different thermodynamic phases holds critical significance in various scientific and industrial domains. Interfaces are pivotal in understanding a wide array of physical phenomena, such as freezing,[1,2] nucleation,[3,4] confinement,[5] as well as multiple technological[6] and biological[7,8] processes. Special focus has been devoted to the study of the solid–liquid interface;[3,9–17] however, it is important to note that its comprehensive study is far from trivial due to its inherent complexity.[9]

One of the pioneering contributions to the thermodynamic understanding of interfaces can be attributed to Gibbs. In his seminal work,[18] he introduced the concept of the interface between two different phases as a zero-width plane, often referred to as the "Gibbs' dividing surface." Gibbs associated this plane with the surplus of thermodynamic properties of the two phases once the interface is formed. Among the different parameters to characterize the properties of an interface, a key quantity is the interfacial free energy (γ), which quantifies the reversible work needed to generate an interface per unit of area. Later, Cahn reformulated this formalism using Cramer's rule so that the excesses of extensive properties are expressed through differential coefficients given by determinants that are composed of extensive properties of the interface.[19] In such a way, there is no need for using the dividing surface.

In the case of liquid–solid interfaces, determining the liquid–solid interfacial free energy (γ_{ls}) is not straightforward generally due to the high computational cost associated with its calculation. As will be formulated later, γ_{ls} cannot be directly measured from a liquid–solid coexisting system and requires more sophisticated approaches to be calculated. One of the methods relies on the measurement of crystal nucleation rates in supercooled fluids. Within the framework of the Classical Nucleation Theory (CNT),[20–22] the estimation of γ_{ls} is possible as a function of the

saturation.[23–30] Another experimental indirect approach consists in measuring the angle a liquid droplet forms with a solid surface.[31,32] However, issues such as evaporation, swelling, or surface imperfections affect accuracy, and the surface must be flat and chemically uniform. Deviations from these ideal conditions cause hysteresis between wetting and dewetting, which leads to non-unique contact angle measurements and makes the Young equation unsuitable for calculating solid–liquid interfacial energy.[33] All the intricacies and necessary approximations in experimental efforts to ascertain the liquid–solid interfacial free energy (γ_{ls})[34–36] underscore the growing significance of numerical approaches through molecular simulations to estimate this quantity. This growing importance is evident in the substantial body of research dedicated to developing and refining different computational methods. In fact, in the past two decades, a multitude of innovative methodologies have emerged in response to this need. Direct measurements of the interfacial free energy can be performed through various techniques, such as cleaving,[37] tethered Monte Carlo,[17] metadynamics,[38] mold integration,[13,39] capillary wave fluctuations,[16] Gibbs–Cahn integration,[40] and other related thermodynamic integration schemes.[41–43] These techniques have demonstrated their capability to yield reliable estimates of the liquid–solid interfacial free energy for various crystallographic planes and a wide array of condensed matter systems.[2,3,10,12,30,44–52] It shall be noted that regardless of their success in the calculation of such an elusive quantity, all existing techniques come with varying degrees of computational cost and implementation complexity.

In this work, we apply the Gibbs–Cahn integration method,[47,53,54] which allows for the determination of the interfacial free energy, γ, along the coexistence line, provided that the value of γ is known for one thermodynamic state. By integrating the Gibbs–Cahn equation (a first-order differential equation), we can determine γ at other points along the coexistence line. This bears some resemblance to the Gibbs–Helmholtz relation,[55] which allows determining the change in chemical potential with temperature. With such a method, the enthalpy is integrated, and therefore, it has to be known along the integration pathway. The accuracy of the Gibbs–Cahn method relies heavily on the precise determination of γ at a single state point. Although we apply this approach for both liquid–solid and liquid–vapor interfaces, the latter case does not strictly require this methodology as there are more direct ways of obtaining γ for liquid–vapor systems. In what follows, we detail the methodology that enables the calculation of γ along the coexistence line using straightforward unbiased simulations.

II. METHODOLOGY

In the Gibbs framework, the dividing surface separates the two bulk phases, and the surface excess quantities represent the deviation of the system's real properties from the properties that would be obtained if the two bulk phases extended uniformly to the interface. In this framework, the excess energy, entropy, and number of particles per surface area for a system of two coexisting phases, 1 and 2, are given by

$$e = (E - \rho_1^E V_1 - \rho_2^E V_2)/A, \quad (1)$$

$$\eta = (S - \rho_1^S V_1 - \rho_2^S V_2)/A, \quad (2)$$

$$\Gamma = (N - \rho_1^N V_1 - \rho_2^N V_2)/A, \quad (3)$$

where e, η, and Γ are the surface excess energy, entropy, and number of particles per surface area, respectively, associated with the presence of an interface. A is the interfacial area and E, S, and N are the total energy, entropy, and number of particles of the system containing both phases in coexistence, respectively. ρ^E, ρ^S, and ρ^N are the bulk densities of energy, entropy, and number of particles, respectively. V is the volume of each phase denoted as 1 and 2. The values of e, η, and Γ depend on the arbitrary choice of the dividing interface. Among all possibilities, the equimolar dividing surface is usually chosen and it is defined as that for which the value of $\Gamma = 0$ (i.e., the surface density of excess molecules is zero).

Alternatively, the formalism of Cahn,[56,57] which builds on the work of Gibbs, uses a layer of finite thickness. In this case, Eqs. (1)–(3) still apply although they correspond to the layer instead of the dividing surface. Cahn uses Cramer's rule to propose a compact thermodynamic description employing determinants of extensive properties.[57] A particular choice of extensive variables makes this approach equivalent to the one of Gibbs for the equimolar dividing surface. By using Cahn's approach in such a form, it was shown in Refs. 47, 53, and 54 that for liquid–solid interfaces, the interfacial free energy dependence along the coexistence line can be obtained from thermodynamic integration schemes. In particular, for a monocomponent system of cubic geometry under hydrostatic stress, the following expression was suggested in Ref. 47:

$$\left[\frac{d(\gamma_g/T)}{dT}\right]_{coex} = -\rho_s(T)^{-2/3}\left[\frac{e(T)}{T^2} + \frac{2\tau(T)}{3\rho_s(T)T}\left(\frac{d\rho_s}{dT}\right)_{coex}\right], \quad (4)$$

which can be integrated to yield

$$\frac{\gamma_g}{T} - \frac{\gamma_{g,0}}{T_0} = -\int_{T_0}^{T}\rho_s(T)^{-2/3}\left[\frac{e(T)}{T^2} + \frac{2\tau(T)}{3\rho_s(T)T}\left(\frac{d\rho_s}{dT}\right)_{coex}\right]dT, \quad (5)$$

where γ_g is the interfacial free energy per surface atom: $\gamma_g = \rho_s^{-2/3}\gamma_{ls}$ (with ρ_s being the solid number density and γ_{ls} being the liquid–solid interfacial free energy) and τ is the interfacial stress, which can be defined[58–60] as

$$\tau = \int_{-\infty}^{\infty}[p_N(x) - p_T(x)]dx = \frac{L_x}{2}(\bar{p}_N - \bar{p}_T), \quad (6)$$

where L_x is the long side of the simulation box (perpendicular to the interfaces in our simulations) and p_N and p_T are the normal and tangential components of the pressure tensor with respect to the interfaces. p_T refers to the average over the two tangential directions. To improve statistics, the tangential component is averaged over the two tangential directions, which are equivalent to each other. Factor 2 accounts for the existence of two interfaces when performing simulations under periodical boundary conditions. Equation (5) is the key equation to solve here: it can be used to predict γ at any temperature T (and pressure along the coexistence line) once a value for the interfacial free energy (γ_0) at a given temperature (T_0) and pressure is calculated. We note that cubic geometry was assumed, which in the case of hexagonal ice is an approximation. Nevertheless, the interfacial free energy of cubic ice is very similar to that of hexagonal ice,[12] so we do not expect this approximation to have any significant effect. Note that all properties of the integrand

of Eq. (5) are computed along the liquid–solid coexistence curve (so that when T changes p changes to the corresponding value of the coexistence curve). A requirement to solve Eq. (5) is to know how the interfacial excess energy (e) depends on T, which can be easily computed through Eq. (1). The energy densities for the bulk phases can be computed by performing NpT simulations of bulk phases 1 and 2 separately. The total energy (E) is obtained from a Direct Coexistence (DC) simulation.[61] DC simulations are performed in the canonical ensemble, and in such simulations, the two coexisting phases are in direct contact forming two interfaces separating them. The volume occupied by each coexisting phase (V_1 and V_2) is easily calculated knowing the coexisting density of each phase (previously calculated through NpT simulations). To do so, we take into account that the layer in the formalism of Cahn is defined by flat planes and that we choose to use it in the form that is equivalent to setting the Gibbs dividing surface at $\Gamma = 0$ [see Eq.(3)] to obtain V_1 and V_2 by solving

$$\left.\begin{array}{r} V = V_1 + V_2 \\ N = \rho_1^N V_1 + \rho_2^N V_2 \end{array}\right\}, \qquad (7)$$

where N and V are input simulation parameters. We stress the fact that it is essential to ensure in DC simulations that the solid crystal lattice is not strained under the imposed temperature and simulation box dimensions (i.e., remains at the equilibrium solid density).

Finally, we need to obtain τ [Eq. (6)] in order to solve Eq. (5). This is another straightforward measurement, directly inferred from the DC simulations, since the pressure tensor can be directly calculated during the simulation. In summary, the present methodology requires performing a small amount of unbiased simulations (NVT DC simulations + bulk crystal and bulk fluid simulations) to obtain the dependence of the interfacial excess energy (e) and the excess interfacial stress (τ) with temperature, and once γ_{ls} is known for a given coexistence point, we can predict the liquid–solid interfacial free energy along the coexistence line.

As discussed in Ref. 62, the described framework is useful for interfaces containing solids. For fluid–fluid interfaces, the same formalism applies but becomes simpler. In particular, Eq. (4) can be rewritten (see the supplementary material) as

$$\left[\frac{d(\gamma/T)}{dT}\right]_{coex} = -\frac{e}{T^2} - (\tau - \gamma)\frac{2}{3\rho_s T}\left(\frac{d\rho_s}{dT}\right)_{coex}. \qquad (8)$$

However, for fluid–fluid interfaces, $\tau = \gamma$, which makes the second term in the right-hand-side zero. While solids may present strained states, such as the stretching or compression of the lattice, fluids do not do so due to their capability to reorganize their structure upon temperature/pressure variations in a given simulation box. That is, for a given thermodynamic state, the fluid–fluid interfaces adapt to reach always the same density but solids can be forced to a different density if their lattice is strained. Another way to see this is that the density of a fluid phase is not a variable of the state of the interfacial system, whereas a solid, which is constrained by its structure, requires this variable to describe the thermodynamic state. Therefore, for liquid–vapor interfaces, the interfacial free energy along the coexistence line can be obtained as

$$\int_{1/T_0}^{1/T} e\left(\frac{1}{T}\right) d\left(\frac{1}{T}\right) = \int_{\gamma_{lv,0}/T_0}^{\gamma_{lv}/T} d\left(\frac{\gamma_{lv}}{T}\right), \qquad (9)$$

which after integrating the expression results in

$$\frac{\gamma_{lv}}{T} = \frac{\gamma_{lv,0}}{T_0} + \int_{1/T_0}^{1/T} e\left(\frac{1}{T}\right)d\left(\frac{1}{T}\right), \qquad (10)$$

where γ_{lv} refers to the liquid–vapor interfacial free energy. $e(1/T)$ denotes dependence on $1/T$ of the excess energy.

In this work, we exploit the thermodynamic integration approach for computing γ along the liquid–solid coexistence line of the Lennard-Jones potential and the mW water model and for the liquid–vapor coexistence line of the Lennard-Jones and TIP4P/2005 water model.

III. SIMULATION DETAILS

We employ the Broughton and Gilmer (BG) truncated Lennard-Jones potential,[37] the atomistic non-polarizable TIP4P/2005 water model,[63] and the mW[64] coarse-grained water model. The potentials for all these models can be found in the supplementary material (Sec. SI). Simulations were performed with the Large-scale Atomic/Molecular Massively Parallel Simulator (LAMMPS)[65] molecular dynamics package for the case of the Lennard Jones and mW potentials and the GROMACS molecular dynamics package[66] (version 4.6.7) for the TIP4P/2005 model.

For the Lennard-Jones BG potential, we fix $\epsilon = 1, \sigma = 1, m = 1$ and use reduced units, indicated with the symbol * (further details can be found in the supplementary material), where $T^* = k_B T/\epsilon$. We perform DC simulations in the NVT ensemble, keeping the temperature constant with the Nosé–Hoover thermostat.[67–69] For the simulations in the NpT ensemble (i.e., bulk liquid or bulk crystal systems), we fix the pressure with the Nosé–Hoover barostat.[67–69] The relaxation times are 1 and 10 (in reduced time units) for the thermostat and barostat, respectively. We integrate the equations of motion using the velocity-Verlet integrator. The simulation time step chosen is 0.001 in reduced time units. We carry out mold integration calculations[13] using the LAMMPS mold package[39] developed by us.

For the simulations of the mW model in LAMMPS, we set the relaxation time of the thermostat and barostat at 0.1 and 0.5 ps, respectively. The simulation time step chosen is 5 fs. The forces calculated using the mW model vanish at a cut-off distance of $r_c = a\sigma = 1.8\sigma$, with $\sigma = 2.3925$ Å being the water molecular diameter as proposed in Ref. 64. The same barostat and thermostat as in the Lennard-Jones BG simulations were used.

For the TIP4P/2005 simulations, we employ GROMACS. The v-rescale (Bussi–Donadio–Parrinello) thermostat[70] is used in both NVT and NpT simulations. For NpT simulations, the Parrinello–Rahman barostat[71] is also used to keep the pressure constant. We integrate the equations of motion using the leap-frog integrator.[72] The simulation time step chosen is 0.002 ps, and the thermostat and barostat relaxation times are 2 and 0.75 ps, respectively. For the TIP4P/2005 potential, we set the cutoff of both dispersive interactions and the real part of the electrostatic interactions at 1.3 nm using a switch radius at 1.2 nm,[73] and no long-range dispersion corrections for energy and pressure are applied. Long-range Coulombic interactions were treated with the Particle-Mesh Ewald (PME) solver.[74,75] We keep the O–H bond length (0.9572 Å) and H–O–H angle (104.52°) values constant with the LINCS algorithm implemented in GROMACS.[76]

IV. RESULTS AND DISCUSSION

A. Thermodynamic integration of γ along the liquid–solid coexistence line of Lennard-Jones particles

We begin by applying the Gibbs–Cahn thermodynamic integration methodology to the study of γ_{ls} along the liquid–solid (face centered cubic, fcc) coexistence line of the Lennard-Jones BG potential. The coexistence line in the $p^* - T^*$ plane indicates the coexistence conditions between the liquid and solid phases. Such a curve is shown in Fig. 1 for the Lennard-Jones BG and mW models, which will be studied later. In order to determine the coexistence conditions, we performed direct coexistence simulations in the NpT ensemble. Further details on how to obtain the coexistence conditions are detailed in Sec. SII of the supplementary material.

We first illustrate the thermodynamic integration methodology for the (110) plane of the fcc phase in the BG model. We prepare a NVT DC simulation containing ~10 000 particles, and we obtain E [to later use it in Eq. (1)], as well as τ from Eq. (6). It is crucial to set the correct box dimensions for NVT DC simulations. Since the

(a) Lennard-Jones BG

• This work
• Davidchack & Laird, JCP (2003)

(b) mW

FIG. 1. Liquid–solid coexistence line in the pressure–temperature plane for (a) the Lennard-Jones system and (b) the mW water model.

coexistence density for the fcc solid is known,[37] we prepare simulation boxes that perfectly accommodate the solid at its equilibrium lattice parameters along the directions tangential to the interface at the chosen temperature—otherwise the solid phase will be stressed, and hence, its chemical potential will be higher than that at the coexisting conditions. We prepare simulation boxes that initially contain the same amount of solid and liquid particles and fix the total density around the average between the equilibrium densities of the respective bulk solid and liquid phases at coexistence conditions. In principle, the choice of the amount of inserted particles of each phase is not relevant since, as long as the global density is between ρ_s and ρ_l, the system will spontaneously equilibrate (and the pressure along the direction perpendicular to the interface matches the coexistence pressure) in order to accommodate the two coexisting phases in equilibrium, regardless of our choice for the initial configuration. Then, in parallel, the bulk simulations are performed for both the liquid and solid phases at the corresponding coexistence conditions using NpT simulations (with systems sizes of ~10 000 particles), from where we obtain ρ_1^E and ρ_2^E. With such information, we obtain the excess interfacial free energy, e, by solving Eq. (1), where A is directly measured from the DC simulation box length ($A = 2*L_y*L_z$) and V_1 and V_2 are obtained from Eq. (7). For the sake of computational efficiency, we use system sizes about ten times smaller than those employed in Ref. 47. In spite of the large system size difference, our results are consistent with those of Ref. 47, suggesting the absence of finite-size effects in our simulations (we note that the shortest dimension in our DC simulations fits at least 12 unit cells, spanning more than five times the cutoff distance). Moreover, using a different technique (metadynamics), in Ref. 38, finite size effects were analyzed in calculations of liquid–solid interfacial free energies and reliable results were obtained for systems even smaller than ours.

In Fig. 2(a), we plot e against T and its linear fit, along with the previously calculated values from Ref. 47. Note that for each temperature, the system is at a different pressure (given by the corresponding coexistence pressure at the imposed temperature). Moreover, in Fig. 2(b), we also plot τ against T, once again comparing it to the results of Laird et al.[47] for the same crystal orientation and Lennard-Jones BG potential. Unless otherwise stated, we perform linear regression due to (1) the fact that, overall, the data we report in this figure and the following ones may follow this trend; (2) the difficulty of assigning a higher degree polynomial fit to data in which we use a limited amount of points (3 in this case); our choice of using linear fits is also justified by the fact that we find a good agreement between the γ_{ls}'s we obtain through integration and those computed with direct estimates.

We now proceed to evaluate Eq. (5). In Fig. 2(c), we show the integrand of the right-hand side term of Eq. (5) as a function of temperature (and implicitly of pressure through the variation along the coexistence line). Here, we apply the thermodynamic integration methodology discussed in Sec. II. As an extension of previous work,[47,77] we have obtained fitted expressions for e, τ, and ρ_s with T. Therefore, we continuously evaluate the integrand of Eq. (5) and solve the equation, which yields a continuous prediction of the integration, while in the originally proposed method, Eq. (5) was discretely evaluated for the states at which DC and bulk simulations were performed, and the integrand was calculated by means of the trapezoidal integration method. Here, we fit the behavior of
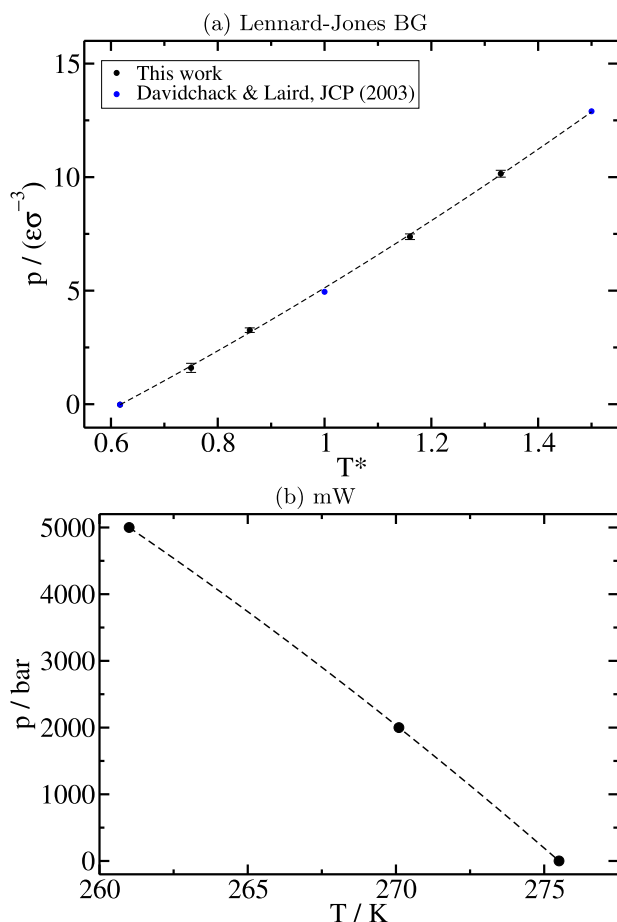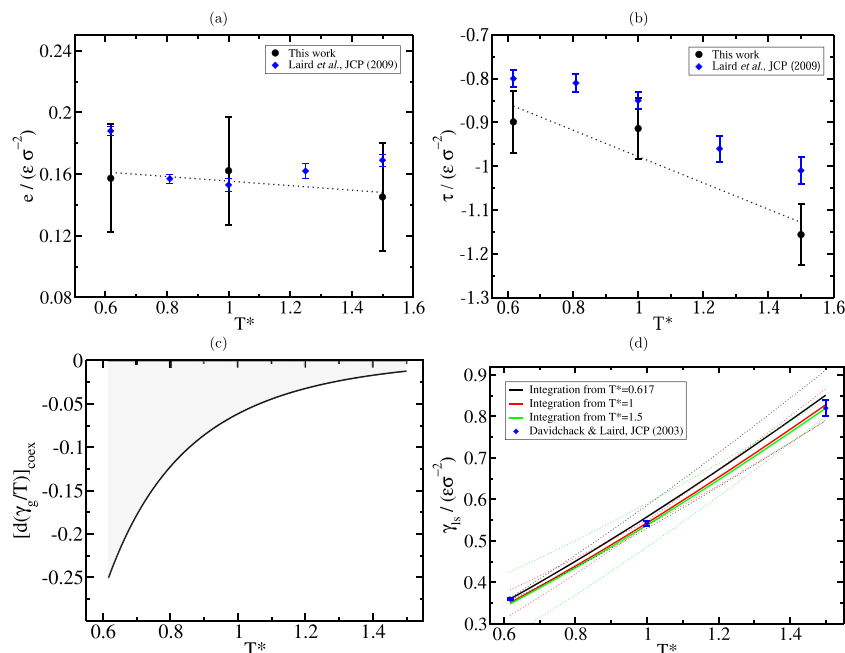
FIG. 2. Gibbs–Cahn integration of γ_{ls} for the BG Lennard-Jones fcc (110) plane: (a) excess interfacial energy as a function of temperature along with the results of Laird et al.[47] The black dashed line represents a linear fit to our data: $e = 0.1702 - 0.01471T^*$ (where $T^* = k_B T/\epsilon$). (b) Excess interfacial stress as a function of temperature, along with the results of Laird et al.[47] The black dashed line represents a linear fit to our data: $\tau = -0.6767 - 0.3012T^*$. (c) Slope of γ_g/T as a function of temperature for the (110) plane along the melting line. The shaded region represents the integral of such a function along temperature. (d) Predicted interfacial free energy as a function of T^* along the coexistence line for the (110) plane. The continuous lines indicate the estimations obtained from Eq. (5) using the γ_{ls} values from Ref. 10 (blue diamonds). Dotted lines indicate the uncertainty limits for each of the estimations from the different states as indicated in the legend.

e, τ, and ρ_s with T through fits (linear for e and τ and second degree for ρ_s unless stated otherwise), as opposed to only evaluating the integrand at the states at which we have directly computed e, τ, and ρ_s. This allows us to easily obtain continuous predictions of γ_{ls} with T in a simple manner, as opposed to integrating using the trapezoidal rule integration method. The dependence of ρ_s against T^* is required, and we obtain an analytical expression for it (second order polynomial fit, Fig. S3). The shaded area depicted in Fig. 2(c) represents the integrated equation (5), and using an integration starting value of the interfacial free energy for a given state point, we obtain the behavior of γ_{ls} against temperature under coexistence conditions [Fig. 2(d)].

We use the reported γ_{ls} values from Ref. 10 as starting points ($\gamma_{ls,0}$ and T_0) for thermodynamic integration. In Fig. 2(d), we show the predicted curves for γ_{ls}. The estimations from the Gibbs–Cahn integration (independently of the starting state point) are in excellent agreement with the individually computed values of γ_{ls} at different temperatures since within the error bars of both the direct estimates and the Gibbs–Cahn predictions, the values obtained from both approaches match. We estimate the uncertainty bounds by combining two sources of error: the error in determining γ_{ls} at the starting integration point (which comes from the technique used to directly determine γ_{ls}) and the error in e and τ, which propagates with temperature. For this second component, we calculate the maximum error in e and τ at the furthest integration point and linearly interpolate this error for intermediate points along the thermodynamic integration pathway. We account for the fact that the error in e and τ is zero at the lower bound of the integration, i.e., at $T = T_0$. The error in e and τ is obtained from block analysis, in which we divide the simulation data into uncorrelated blocks that are averaged each of them. Then, the error is obtained as the standard deviation of the different blocks over the square root of the number of blocks.

This is later multiplied by a t-student value for a 95% confidence level to finally obtain the error in e and τ.

Next, we apply this methodology to the (100) and (111) fcc crystal planes. In Fig. 3, we show the predicted γ_{ls} from thermodynamic integration along with direct calculations of γ_{ls} using the cleaving method[10] and mold integration (this work). We once again obtain a good prediction of the interfacial free energy (the predictions from Gibbs–Cahn integration match with direct calculations within the error limits), this time using our own estimates of γ_{ls} as reference values for the integration (see Sec. SIII of the supplementary material for details on our calculations of γ_{ls} through the mold integration technique). Similar to Ref. 47, the results for the (111) plane have a greater deviation from the calculated γ_{ls} than those for the (110) and (100) planes: the black curve in Fig. 2(d) for the (110) plane deviates $0.03\epsilon/\sigma^2$ and the black curve in Fig. 3(b) deviates $0.05\epsilon/\sigma^2$ for the (111) one. These greater deviations of γ_{ls} only appear when the target temperature changes by a factor of 2.5 the reference temperature from which the integration is performed. In this aforementioned example, the prediction is evaluated at $T^* = 1.5$ when the integration begins at $T^* = 0.617$.

Additionally, we show all the individual fits for e and τ as a function of T^* for the (110) and (111) planes plotted in Fig. 4. Furthermore, we provide the data for e at each temperature for the three studied planes in Table I. As can be attained from such e and τ data, all the values follow a monotonic trend along the coexistence line. It is remarkable how the interfacial stress is much lower for the case of the (100) plane [and even goes from negative to positive values, Fig. 4(c)], while it is not negligible for the (110) and (111) planes. This reduces the uncertainty in integration since the second term in the right-hand side of Eq. (5) contributes very small values to the prediction of γ_{ls} along the coexistence line. It is also notable how the difference in the uncertainty obtained for e and τ obtained from
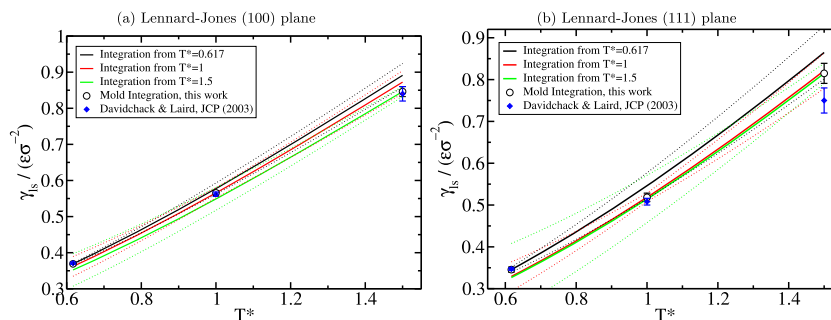
FIG. 3. Predicted interfacial free energy as a function of T^* along the coexistence line for (a) the (100) Lennard-Jones plane and (b) the (111) Lennard-Jones plane of the fcc crystal phase. The continuous lines indicate the predictions obtained from Eq. (5) using the mold integration calculations as integration limits, while the dashed lines depict the uncertainty limits for each of the estimations from different temperatures. We also plot the direct calculations of γ from Ref. 10 using the cleaving technique. Note that for both planes, the mold integration γ_{ls} and those from Ref. 10 overlap, except the one at the highest T^* for the (111) plane.

TABLE I. e and τ data for all of the different states considered in this study for the Lennard-Jones system.

	T^*	(100)	(110)	(111)
$e/(\epsilon\,\sigma^{-2})$	0.617	0.11(3)	0.16(4)	0.16(4)
	1	0.05(3)	0.16(4)	0.13(4)
	1.5	−0.01(3)	0.15(4)	0.11(4)
$\tau/(\epsilon\,\sigma^{-2})$	0.617	−0.23(4)	−0.90(7)	−0.88(8)
	1	−0.04(4)	−0.92(7)	−1.20(8)
	1.5	0.23(4)	−1.17(7)	−1.31(8)

DC simulations differs between our calculations and those from Ref. 47, which are plotted along with our results in Fig. 2. In our calculations, we directly estimate the error bar from the standard deviation along the simulation. This discrepancy may arise from the fact that the system sizes used in Ref. 47 are about an order of magnitude greater, as well as the possibility of performing even more computationally intensive simulations, although the length of the simulations was not specified in Ref. 47. Moreover, we provide a direct comparison of our results, with those from Ref. 47. To perform Gibbs–Cahn integration with such data, we fitted the τ values provided in Ref. 47 with second order polynomial fits as the trend of that data suggests. In Figs. S5–S7 of the supplementary material, we probe how the difference between our results and those from Ref. 47 is minimal, and our results are only quantitatively less accurate for the (111) plane, despite the overall larger uncertainty in the determination in e and τ.

We independently estimate the interfacial free energy of the three different states studied here ($T^* = 0.617$, $T^* = 1$, $T^* = 1.5$), which are the same as those evaluated in Ref. 10. For this purpose, we perform Mold Integration (MI) calculations (see supplementary material, Sec. SIII for further details on this technique and calculations). We plot our γ_{ls} values from Mold Integration (black circles filled in white) along with those from Ref. 10 (blue diamonds) in Fig. 3. Overall, we find excellent agreement between our calculations and those from Ref. 10 for all the cases except for the (111) plane at $T^* = 1.5$, for which we obtain a moderately higher value. Interestingly, the value obtained from Mold Integration is

in better agreement with our estimations from the Gibbs–Cahn thermodynamic integration than with the Cleaving values from Ref. 10, especially with the fit obtained from $T^* = 1$ [red curve in Fig. 3(b)]. It must be noted that unlike for the case of the (110) plane (where γ_{ls} values were taken from Ref. 10), for the (100) and (111) planes, we use MI values as integration starting points (γ_0, and T_0) to solve Eq. (5).

The predictions from thermodynamic integration yield results that overlap with those directly evaluated within the error bars [Figs. 2(d) and 3]; however, the deviation becomes larger for values estimated from very distant temperatures. We find that in the Lennard-Jones system, all the γ_{ls} thermodynamic integration predictions match with the directly measured values for the three studied planes [Figs. 2(d) and 3].

B. Thermodynamic integration of γ for the mW water model along its melting line

We now proceed to test the Gibbs–Cahn integration methodology along the liquid–solid coexistence line of a more complex case, the mW coarse-grained water model. This monoatomic model reproduces the behavior of water because the tetrahedral coordination of the atoms is favored by adding a three-body term that penalizes non-tetrahedral coordinations (see the supplementary material). We aim to predict γ_{ls} for the ice Ih basal (0001) plane, for which previous calculations of Espinosa et al.[2] using mold integration have already established the dependence of γ_{ls} with T along the melting line. Analogous to the BG Lennard-Jones case, we perform independent NVT DC and NpT bulk simulations in order to obtain the dependence of e, τ, and ρ_s with temperature, and later solve Eq. (5), using the values from Ref. 2 as starting points for the integration [$\gamma_{ls,0}$ and T_0 in Eq. (5)].

In Fig. 5, we show the results of γ_{ls} from thermodynamic integration for the mW model. We observe that the Gibbs–Cahn integration is able to describe the change of interfacial free energy with temperature along the coexistence line. We find that the curvature of γ_{ls} with T deviates from a linear trend in a more pronounced way than for the BG Lennard-Jones system [see Figs. 2(d) and 3] and the value of γ_{ls} decreases with T (for the temperature range studied here). The fact that the Gibbs–Cahn integration predicts
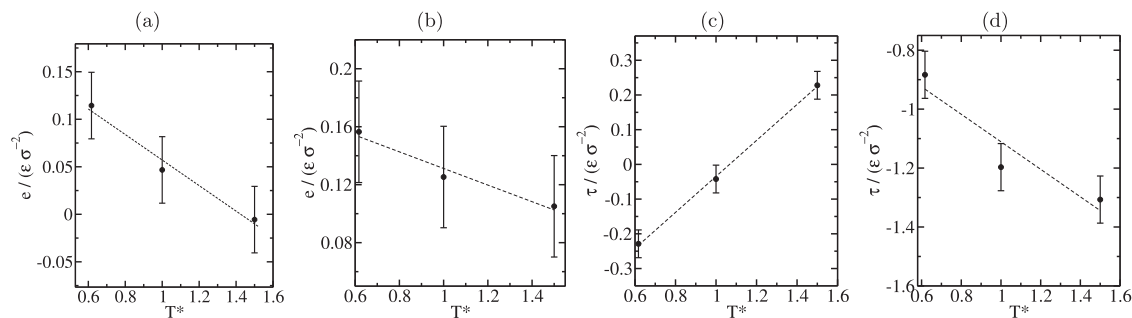
FIG. 4. Surface excess energy as a function of temperature for the Lennard-Jones liquid–solid interface of the (100) (a) and (111) (b) planes. Interfacial stress as a function of temperature for the Lennard-Jones liquid–solid interface of the (100) (c) and (111) (d) planes.
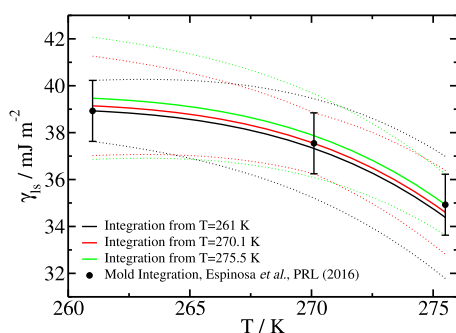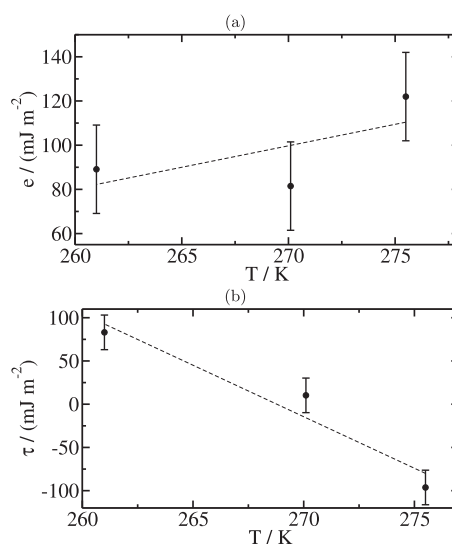

FIG. 5. Predicted interfacial free energy against temperature (along the melting line) from Gibbs–Cahn integration [Eq. (5)] for the ice Ih basal plane of the mW water model. Direct calculations of γ_{ls} using mold integration[2] (black circles) have been taken as integration limits.

FIG. 6. (a) Surface excess energy (e) against T for the ice Ih-fluid of the mW water model with the crystal phase exposing the basal plane to the liquid. (b) Interfacial stress (τ) against T for the ice Ih-fluid of the mW water model with the crystal phase exposing the basal plane to the liquid.

this behavior proves the power of this approach to quantify the dependence of the interfacial free energy along a coexistence line. This is of great relevance for the case of solid–liquid interfaces, where γ_{ls} calculations are challenging, and the implementation of advanced simulation techniques is required.[13,16,17,37–39,41,42] For the mW model, the e and τ fits are shown in Fig. 6, and the corresponding data can also be found in Table II. From Fig. 6, it can be seen that different from the case of the Lennard-Jones system, e increases with temperature. The interplay between increasing e and decreasing τ along the coexistence line for this temperature range yields the singular trend of the interfacial free energy that, apart from direct measurements, can be recovered using the Gibbs–Cahn integration method.

C. Thermodynamic integration of γ along the liquid–vapor coexistence line

Estimating the liquid–vapor interfacial free energy (γ_{lv}) along the coexistence line is considerably simpler than it is for the liquid–solid interface. By means of a DC simulation containing the two coexisting phases in the NVT ensemble, γ_{lv} can be determined through the relation

$$\gamma_{lv} = \frac{L_x}{2}(\bar{p}_N - \bar{p}_T). \quad (11)$$

Nevertheless, as a proof of concept, we apply here the Gibbs–Cahn thermodynamic integration method to show how γ_{lv} can be also easily determined along the coexistence line with a

TABLE II. e and τ values for all of the different states considered in this study for the ice Ih basal plane of the mW water model.

	T (K)	P (bar)	e (mJ m^{-2})	τ (mJ m^{-2})
Ice Ih mW	275.5	1	122(20)	−96(20)
	270.1	2000	81(20)	10(20)
	261	5000	89(20)	83(20)
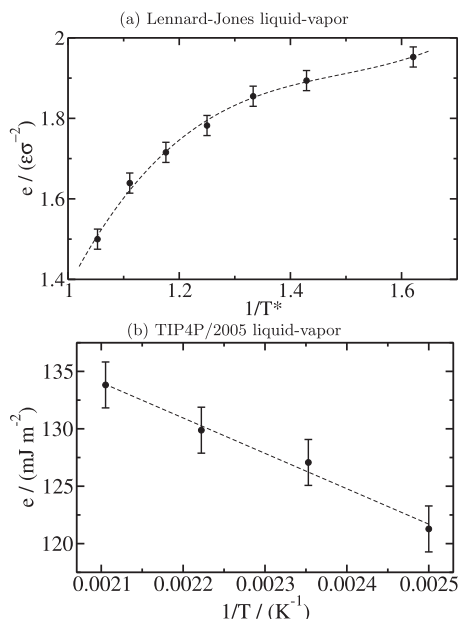
FIG. 7. (a) Surface excess energy (e) against the inverse of temperature (at the corresponding coexisting pressure for each temperature) for the Lennard-Jones liquid–vapor interface. Filled points are direct estimations, while the dashed line indicates the fit to the data. In this case, to better follow the trend, a third order polynomial fit was used. (b) e against the inverse of temperature for the TIP4P/2005 water model liquid–vapor interface. Filled points are direct estimations of e, while the dashed line depicts the linear fit to the obtained data.

TABLE III. Surface excess energy (e) values for the Lennard-Jones liquid–vapor interface at the different temperatures studied.

T^*	$e/(\epsilon\,\sigma^{-2})$
0.617	1.952(25)
0.7	1.894(25)
0.75	1.855(25)
0.8	1.782(25)
0.85	1.715(25)
0.9	1.639(25)
0.95	1.500(25)

TABLE IV. Surface excess energy (e) values for the TIP4P/2005 liquid–vapor interface at the different temperatures studied.

T (K)	e (mJ m^{-2})
400	121(2)
425	127(2)
450	130(2)
475	134(2)

similar approach as that shown for liquid–solid interfaces. For this goal, one needs to compute the excess interfacial energy along temperature at coexisting conditions [Eq. (10)]. We then proceed by first performing liquid–vapor DC simulations in the canonical ensemble, from which we obtain E, as well as the coexistence pressure at the fixed temperature. Once we know the coexistence pressure, we perform NpT simulations of the bulk liquid and vapor phases under such conditions separately in order to obtain ρ^E for both phases, which with the use of Eq. (1) we obtain e. We can then fit e as a function of the inverse of temperature, which will be integrated [Eq. (10)]. In this case, the integration limit conditions [γ_0 at T_0 in Eq. (10)] are also extracted from NVT DC simulations applying the Kirkwood–Buff equation [Eq. (11)]. This equation is equivalent to Eq. (6) used in liquid–solid equilibrium to compute the excess interfacial stress.[62]

We perform the aforementioned simulations for the BG Lennard-Jones system and the TIP4P/2005 water model and then make use of thermodynamic integration [Eq. (10)] to predict γ_{lv} along the coexistence line. We show the employed e against $1/T$ fits in Fig. 7, as well as include the e values for each temperature in Tables III and IV (for the Lennard Jones and TIP4P/2005 models, respectively). Our e calculations for the TIP4P/2005 model are in good agreement with those from Hrahsheh *et al.*[78] since we perfectly capture the trend obtained from single-state calculations. In Fig. 8(a), we show how the integration method for the BG Lennard-Jones potential yields very accurate predictions of γ_{lv} with temperature, independent of the starting integration temperature.

We also show that for the TIP4P/2005 [Fig. 8(b)], the prediction of γ_{lv} from the different states also provides accurate interfacial free energies along the coexistence line. These results show that only the interfacial energy, e, is needed to determine the change in γ_{lv} across liquid-vapor coexistence lines [as shown by Eq. (10)]. We also clarify that since we are using a truncated TIP4P/2005 potential, we underestimate the critical point and, consequently, the interfacial free energy values[79–81] that we report in this work. Nonetheless, our calculations are consistent since all our simulations are performed under the same approximations, and the direct and indirect estimates of γ_{lv} reach excellent agreement.

It must be noted here that the application of the thermodynamic integration scheme to predict liquid–vapor interfacial free energies along the coexistence line is not an efficient method since in order to provide a prediction of γ_{lv}, one must perform NVT DC simulations at the states that will be later inferred. However, by doing these simulations, γ_{lv} can already be obtained from Eq. (11), making the subsequent integration calculations irrelevant. Nevertheless, these calculations show how this framework is also valid for liquid–vapor interfaces.

D. Evaluation of thermodynamic integration equations

As it has been previously argued,[62] the expressions, methods, and complexity to estimate the interfacial free energy for liquid–vapor and liquid–solid interfaces are completely different. For the case of liquid–vapor interfaces, the calculation is straightforward and can be carried out by using Eq. (11). However, we note that the interfacial free energy in liquid–solid interfaces cannot be calculated through such a relation[62] rather than through specialized simulation techniques.[13,16,17,37–39,41,42] Here, we illustrate how γ_{ls} should not be obtained through Eq. (11). In Fig. 9, we plot both γ_{ls} and τ along the liquid–solid coexistence line (plotted as a function
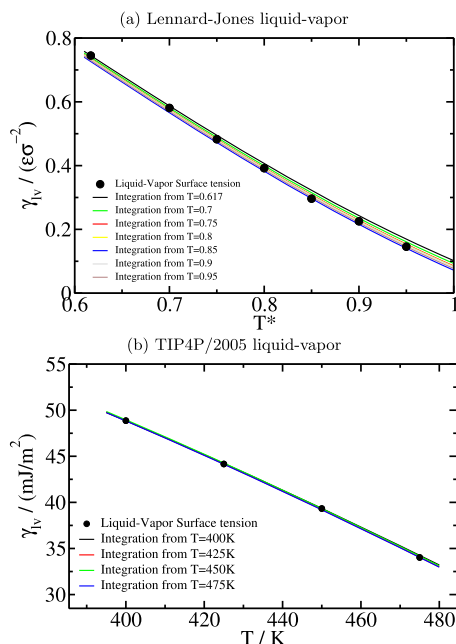
FIG. 8. (a) Interfacial free energy against temperature along the BG Lennard-Jones liquid–vapor coexistence line as predicted through thermodynamic integration [Eq. (10)] from the states indicated in the legend. Direct calculations of γ_{lv} through Eq. (11) are also included as black circles. (b) Interfacial free energy against temperature along the TIP4P/2005 water model liquid–vapor coexistence line. Thermodynamic integration estimates are represented by curves, whereas direct calculations of γ_{lv} are represented by black circles.
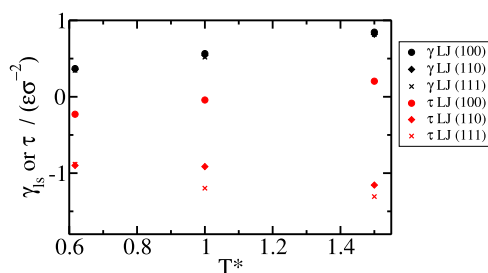
FIG. 9. Liquid–solid interfacial free energy (γ_{ls}) and interfacial stress (τ) as a function of temperature for the different orientations studied (as indicated in the legend) with the Lennard-Jones BG potential. The interfacial free energy values are calculated by us through mold integration calculations, except the (110) orientation, which is taken from Ref. 10.

of the temperature) for the different crystal planes studied with the BG Lennard-Jones potential. It is evident that the two quantities do not match. In fact, the interfacial stress takes negative values for most of the states and orientations we examined, which is unphysical (γ_{ls} must be positive, otherwise demixing into two phases would not occur).

Figure 9 highlights the importance of employing an adequate thermodynamic derivation or simulation method to attain reliable

interfacial free energies for a given system. Since this is a fundamental conceptual error, the community should not use Eq. (11) to determine the interfacial free energy between a fluid and a solid.[62,82] As can be seen in Fig. 9, that could even lead to negative values of the interfacial free energy, which is, of course, an incorrect result. Note that although γ changes at most by about ten percent from one plane to another (at least for the LJ system), values of τ change dramatically from one plane to another. The plane (hkl) dependence of γ is small, whereas the plane (hkl) dependence of τ is huge. This means that one could find crystal orientations for which the stress (τ) is almost zero [for instance the plane 100 of the LJ system shown in Fig. 4(c)]. For these particular planes, one can neglect the τ contribution in Eq. (4) (i.e., omitting the second term of the square bracket) to elucidate the change of γ along the coexistence curve (thus will introduce only a small error) to facilitate a rather simple physical (although approximate) interpretation of the changes of γ_{ls} along the coexistence curve in terms of the surface excess energy e. In retrospect, this is probably what happened in our previous work[83] with the basal plane of ice Ih and Eq. (10) to provide a simple explanation of the origin of a minimum in the ice–water interfacial free energy.

V. CONCLUSION

In this work, we apply a robust thermodynamic integration approach for predicting interfacial free energies along coexistence lines, focusing on liquid–solid and liquid–vapor interfaces. The approach employs molecular dynamics simulations as a working tool, and it streamlines the calculation of γ along coexistence lines by requiring just one initial calculation of this quantity at a reference state. Gibbs–Cahn thermodynamic integration stands as a valuable tool for characterizing one of the most critical quantities in phase transitions—the interfacial free energy—across a wide range of conditions, effectively bypassing the computational challenges and cost associated with traditional techniques for the liquid–solid interface.[3,10,84]

By successfully predicting the interfacial free energy for both liquid–solid (with Lennard-Jones and the mW model) and liquid–vapor (with Lennard-Jones and the TIP4P/2005 model) interfaces, we have demonstrated the method's versatility, making it suitable for a wide array of materials and conditions. We distinguish between interfaces with and without solid phases, which makes the thermodynamic route to predict γ along a coexistence line different. The computational efficiency and accuracy of the method are evident from our results, which consistently agree with other computational techniques that provide direct estimates of γ.

The potential applications of γ predictions through thermodynamic integration are diverse, spanning multiple scientific disciplines, including materials science, chemistry, and physics,[85–88] and complement other thermodynamic pathways for single-state point calculations of γ_{ls}.[13,42,47,48]

SUPPLEMENTARY MATERIAL

See the supplementary material for additional information on the Lennard-Jones, mW, and TIP4P/2005 potentials, as well as an

explanation of the direct coexistence method, our mold integration calculation results, the Lennard-Jones and mW equations of state, a proof for Eq. (9), and a direct comparison between our thermodynamic integration predictions and those from Ref. 47.

AUTHOR DECLARATIONS

Conflict of Interest

The authors have no conflicts to disclose.

Author Contributions

Ignacio Sanchez-Burgos: Data curation (equal); Formal analysis (equal); Investigation (equal); Project administration (equal); Resources (equal); Software (equal); Validation (equal); Writing – original draft (equal); Writing – review & editing (equal). **Pablo Montero de Hijes**: Conceptualization (equal); Investigation (equal); Validation (equal); Writing – original draft (supporting); Writing – review & editing (equal). **Eduardo Sanz**: Conceptualization (equal); Funding acquisition (supporting); Investigation (equal); Methodology (equal); Supervision (supporting); Validation (equal); Writing – review & editing (equal). **Carlos Vega**: Conceptualization (equal); Funding acquisition (supporting); Investigation (equal); Methodology (equal); Supervision (supporting); Validation (equal); Writing – review & editing (equal). **Jorge R. Espinosa**: Conceptualization (equal); Funding acquisition (lead); Investigation (equal); Methodology (equal); Project administration (lead); Resources (lead); Supervision (lead); Validation (equal); Writing – original draft (supporting); Writing – review & editing (equal).

DATA AVAILABILITY

The data that support the findings of this study are available within the article and its supplementary material.

REFERENCES

[1] Y. Zhang, E. Anim-Danso, S. Bekele, and A. Dhinojwala, "Effect of surface energy on freezing temperature of water," ACS Appl. Mater. Interfaces **8**(27), 17583–17590 (2016).

[2] J. R. Espinosa, A. Zaragoza, P. Rosales-Pelaez, C. Navarro, C. Valeriani, C. Vega, and E. Sanz, "Interfacial free energy as the key to the pressure-induced deceleration of ice nucleation," Phys. Rev. Lett. **117**(13), 135702 (2016).

[3] I. Sanchez-Burgos, E. Sanz, C. Vega, and J. R. Espinosa, "Fcc vs. hcp competition in colloidal hard-sphere nucleation: On their relative stability, interfacial free energy and nucleation rate," Phys. Chem. Chem. Phys. **23**(35), 19611–19626 (2021).

[4] C. Hoose and O. Möhler, "Heterogeneous ice nucleation on atmospheric aerosols: A review of results from laboratory experiments," Atmos. Chem. Phys. **12**(20), 9817–9854 (2012).

[5] J. C. Rasaiah, S. Garde, and G. Hummer, "Water in nonpolar confinement: From nanotubes to proteins and beyond," Annu. Rev. Phys. Chem. **59**, 713–740 (2008).

[6] M. Asta, C. Beckermann, A. Karma, W. Kurz, R. Napolitano, M. Plapp, G. Purdy, M. Rappaz, and R. Trivedi, "Solidification microstructures and solid-state parallels: Recent developments, future directions," Acta Mater. **57**(4), 941–971 (2009).

[7] A. Cochard, M. Garcia-Jove Navarro, L. Piroska, S. Kashida, M. Kress, D. Weil, and Z. Gueroui, "RNA at the surface of phase-separated condensates impacts their size and number," Biophys. J. **121**(9), 1675–1690 (2022).

[8] I. Sanchez-Burgos, J. A. Joseph, R. Collepardo-Guevara, and J. R. Espinosa, "Size conservation emerges spontaneously in biomolecular condensates formed by scaffolds and surfactant clients," Sci. Rep. **11**(1), 15241–15310 (2021).

[9] R. Bahadur, L. M. Russell, and S. Alavi, "Surface tensions in NaCl–water–air systems from MD simulations," J. Phys. Chem. B **111**(41), 11989–11996 (2007).

[10] R. L. Davidchack and B. B. Laird, "Direct calculation of the crystal–melt interfacial free energies for continuous potentials: Application to the Lennard-Jones system," J. Chem. Phys. **118**(16), 7651–7657 (2003).

[11] R. L. Davidchack and B. B. Laird, "Direct calculation of the hard-sphere crystal/melt interfacial free energy," Phys. Rev. Lett. **85**(22), 4751 (2000).

[12] M. Ambler, B. Vorselaars, M. P. Allen, and D. Quigley, "Solid–liquid interfacial free energy of ice Ih, ice Ic, and ice 0 within a mono-atomic model of water via the capillary wave method," J. Chem. Phys. **146**(7), 074701 (2017).

[13] J. Espinosa, C. Vega, and E. Sanz, "The mold integration method for the calculation of the crystal-fluid interfacial free energy from simulations," J. Chem. Phys. **141**(13), 134709 (2014).

[14] J. R. Espinosa, C. Vega, and E. Sanz, "Ice–water interfacial free energy for the TIP4P, TIP4P/2005, TIP4P/Ice, and mW models as obtained from the mold integration technique," J. Phys. Chem. C **120**(15), 8068–8075 (2016).

[15] B. Cheng, G. A. Tribello, and M. Ceriotti, "Solid–liquid interfacial free energy out of equilibrium," Phys. Rev. B **92**(18), 180102 (2015).

[16] J. Hoyt, M. Asta, and A. Karma, "Method for computing the anisotropy of the solid–liquid interfacial free energy," Phys. Rev. Lett. **86**(24), 5530 (2001).

[17] L. Fernández, V. Martin-Mayor, B. Seoane, and P. Verrocchio, "Equilibrium fluid-solid coexistence of hard spheres," Phys. Rev. Lett. **108**(16), 165701 (2012).

[18] J. W. Gibbs, *Collected Works Longmans* (Green and Co., New York, 1928).

[19] W. C. Johnson and J. M. Blakely, *Interfacial Segregation: Papers Presented at a Seminar of The Materials Science Division of The American Society For Metals, October 22 and 23, 1977* (American Society of Civil Engineers, 1979).

[20] D. Turnbull, "Formation of crystal nuclei in liquid metals," J. Appl. Phys. **21**(10), 1022–1028 (1950).

[21] M. Volmer and A. Weber, "Keimbildung in übersättigten gebilden," Z. Phys. Chem. **119U**(1), 277–301 (1926).

[22] R. Becker and W. Döring, "Kinetische behandlung der keimbildung in übersättigten dämpfen," Ann. Phys. **416**(8), 719–752 (1935).

[23] B. N Hale, "Monte Carlo calculations of effective surface tension for small clusters," Aust. J. Phys. **49**(2), 425–434 (1996).

[24] P. M. Piaggi, J. Weis, A. Z. Panagiotopoulos, P. G. Debenedetti, and R. Car, "Homogeneous ice nucleation in an ab initio machine-learning model of water," Proc. Natl. Acad. Sci. U. S. A. **119**(33), e2207294119 (2022).

[25] I. Sanchez-Burgos, A. R. Tejedor, C. Vega, M. M. Conde, E. Sanz, J. Ramirez, and J. R. Espinosa, "Homogeneous ice nucleation rates for mW and TIP4P/ICE models through lattice mold calculations," J. Chem. Phys. **157**(9), 094503 (2022).

[26] J. R. Espinosa, C. Vega, C. Valeriani, and E. Sanz, "Seeding approach to crystal nucleation," J. Chem. Phys. **144**(3), 034501 (2016).

[27] J. Espinosa, C. Navarro, E. Sanz, C. Valeriani, and C. Vega, "On the time required to freeze water," J. Chem. Phys. **145**(21), 211922 (2016).

[28] C. P Lamas, J. R Espinosa, M. M Conde, J. Ramírez, P. Montero de Hijes, E. G Noya, C. Vega, and E. Sanz, "Homogeneous nucleation of NaCl in supersaturated solutions," Phys. Chem. Chem. Phys. **23**(47), 26843–26852 (2021).

[29] A. Garaizar, T. Higginbotham, I. Sanchez-Burgos, A. R. Tejedor, E. Sanz, and J. R. Espinosa, "Alternating one-phase and two-phase crystallization mechanisms in octahedral patchy colloids," J. Chem. Phys. **157**(13), 134501 (2022).

[30] U. O. M. Vázquez, W. Shinoda, P. B. Moore, C.-c. Chiu, and S. O. Nielsen, "Calculating the surface tension between a flat solid and a liquid: A theoretical and computer simulation study of three topologically different methods," J. Math. Chem. **45**, 161–174 (2009).

[31] T. Young, "III. An essay on the cohesion of fluids," Philos. Trans. R. Soc. London **95**(95), 65–87 (1805).

[32] D. Y. Kwok and A. W. Neumann, "Contact angle measurement and contact angle interpretation," Adv. Colloid Interface Sci. **81**(3), 167–249 (1999).

[33] H. Cha, J. Ma, Y. S. Kim, L. Li, L. Sun, J. Tong, and N. Miljkovic, "*In situ* droplet microgoniometry using optical microscopy," Acs Nano **13**(11), 13343–13353 (2019).

[34] H.-S. Na, S. Arnold, and A. S. Myerson, "Cluster formation in highly supersaturated solution droplets," J. Cryst. Growth **139**(1–2), 104–112 (1994).

[35] H. R. Pruppacher, "A new look at homogeneous ice nucleation in supercooled water drops," J. Atmos. Sci. **52**(11), 1924–1933 (1995).

[36] L. Ickes, A. Welti, C. Hoose, and U. Lohmann, "Classical nucleation theory of homogeneous freezing of water: Thermodynamic and kinetic parameters," Phys. Chem. Chem. Phys. **17**(8), 5514–5537 (2015).

[37] J. Q. Broughton and G. H. Gilmer, "Molecular dynamics investigation of the crystal–fluid interface. VI. Excess surface free energies of crystal–liquid systems," J. Chem. Phys. **84**(10), 5759–5768 (1986).

[38] S. Angioletti-Uberti, M. Ceriotti, P. D. Lee, and M. W. Finnis, "Solid–liquid interface free energy through metadynamics simulations," Phys. Rev. B **81**(12), 125416 (2010).

[39] A. R. Tejedor, I. Sanchez-Burgos, E. Sanz, C. Vega, F. J. Blas, R. L. Davidchack, N. D. Pasquale, J. Ramirez, and J. R. Espinosa, "Mold: A LAMMPS package to compute interfacial freeenergies and nucleation rates," J. Open Source Softw. **9**(95), 6083 (2024).

[40] J. W. Cahn, W. Johnson, and J. Blakely, "Interfacial segregation," in *Proceedings of 1977 ASM Seminar (ASM, Metal Park, OH)* (American Society for Metals, 1979), p. 1.

[41] R. Benjamin and J. Horbach, "Crystal–liquid interfacial free energy via thermodynamic integration," J. Chem. Phys. **141**(4), 044715 (2014).

[42] M. Bültmann and T. Schilling, "Computation of the solid–liquid interfacial free energy in hard spheres by means of thermodynamic integration," Phys. Rev. E **102**(4), 042123 (2020).

[43] F. Leroy, D. J. Dos Santos, and F. Müller-Plathe, "Interfacial excess free energies of solid–liquid interfaces by molecular dynamics simulation and thermodynamic integration," Macromol. Rapid Commun. **30**(9–10), 864–870 (2009).

[44] R. L. Davidchack, "Hard spheres revisited: Accurate calculation of the solid–liquid interfacial free energy," J. Chem. Phys. **133**(23), 234701 (2010).

[45] M. Asta, J. Hoyt, and A. Karma, "Calculation of alloy solid–liquid interfacial free energies from atomic-scale simulations," Phys. Rev. B **66**(10), 100101 (2002).

[46] I. Sanchez-Burgos and J. R. Espinosa, "Direct calculation of the interfacial free energy between NaCl crystal and its aqueous solution at the solubility limit," Phys. Rev. Lett. **130**(11), 118001 (2023).

[47] B. B. Laird, R. L. Davidchack, Y. Yang, and M. Asta, "Determination of the solid–liquid interfacial free energy along a coexistence line by Gibbs–Cahn integration," J. Chem. Phys. **131**(11), 114110 (2009).

[48] B. B. Laird and R. L. Davidchack, "Calculation of the interfacial free energy of a fluid at a static wall by Gibbs–Cahn integration," J. Chem. Phys. **132**(20), 204101 (2010).

[49] J. R. Espinosa, C. Vega, C. Valeriani, and E. Sanz, "The crystal-fluid interfacial free energy and nucleation rate of NaCl from different simulation methods," J. Chem. Phys. **142**(19), 194709 (2015).

[50] Y. Mu and X. Song, "Crystal-melt interfacial free energies of hard-dumbbell systems," Phys. Rev. E **74**(3), 031611 (2006).

[51] J. Liu, R. Davidchack, and H. Dong, "Molecular dynamics calculation of solid–liquid interfacial free energy and its anisotropy during iron solidification," Comput. Mater. Sci. **74**, 92–100 (2013).

[52] A. R. Nair and S. P. Sathian, "A molecular dynamics study to determine the solid–liquid interfacial tension using test area simulation method (TASM)," J. Chem. Phys. **137**(8), 084702 (2012).

[53] T. Frolov and Y. Mishin, "Solid–liquid interface free energy in binary systems: Theory and atomistic calculations for the (110) Cu–Ag interface," J. Chem. Phys. **131**(5), 054702 (2009).

[54] T. Frolov and Y. Mishin, "Temperature dependence of the surface free energy and surface stress: An atomistic calculation for Cu(110)," Phys. Rev. B **79**(4), 045430 (2009).

[55] H. von Helmholtz, *Die Thermodynamik chemischer Vorgänge* (Royal Prussian Academy of Sciences, 1882).

[56] J. W. Cahn, *Thermodynamics of Solid and Fluid Surfaces*, *Interfacial Segregation* (American Society for Metals, 1978), Vol. 2, pp. 3–23.

[57] R. F. Sekerka, *Thermal Physics: Thermodynamics and Statistical Mechanics for Scientists and Engineers* (Elsevier, 2015).

[58] J. G. Kirkwood and F. P. Buff, "The statistical mechanical theory of surface tension," J. Chem. Phys. **17**(3), 338–343 (1949).

[59] J. Alejandre, D. J. Tildesley, and G. A. Chapela, "Molecular dynamics simulation of the orthobaric densities and surface tension of water," J. Chem. Phys. **102**(11), 4574–4583 (1995).

[60] E. de Miguel and G. Jackson, "The nature of the calculation of the pressure in molecular simulations of continuous models from volume perturbations," J. Chem. Phys. **125**(16), 164109 (2006).

[61] A. J. Ladd and L. V. Woodcock, "Triple-point coexistence properties of the Lennard-Jones system," Chem. Phys. Lett. **51**, 155–159 (1977).

[62] N. Di Pasquale and R. L. Davidchack, "Shuttleworth equation: A molecular simulations perspective," J. Chem. Phys. **153**(15), 154705 (2020).

[63] J. L. F. Abascal and C. Vega, "A general purpose model for the condensed phases of water: TIP4P/2005," J. Chem. Phys. **123**(23), 234505 (2005).

[64] V. Molinero and E. B. Moore, "Water modeled as an intermediate element between carbon and silicon," J. Phys. Chem. B **113**(13), 4008–4016 (2009).

[65] S. Plimpton, "Fast parallel algorithms for short-range molecular dynamics," J. Comput. Phys. **117**, 1–19 (1995).

[66] H. Bekker, H. Berendsen, E. Dijkstra, S. Achterop, R. Vondrumen, D. Vanderspoel, A. Sijbers, H. Keegstra, and M. Renardus, "Gromacs: A parallel computer for molecular-dynamics simulations," in *4th International Conference on Computational Physics (PC 92)* (World Scientific Publishing, 1993), pp. 252–256.

[67] S. Nosé, "A unified formulation of the constant temperature molecular dynamics methods," J. Chem. Phys. **81**(1), 511–519 (1984).

[68] W. G. Hoover, "Canonical dynamics: Equilibrium phase-space distributions," Phys. Rev. A **31**, 1695–1697 (1985).

[69] W. G. Hoover, "Constant-pressure equations of motion," Phys. Rev. A **34**(3), 2499 (1986).

[70] G. Bussi, D. Donadio, and M. Parrinello, "Canonical sampling through velocity rescaling," J. Chem. Phys. **126**(1), 014101 (2007).

[71] M. Parrinello and A. Rahman, "Polymorphic transitions in single crystals: A new molecular dynamics method," J. Appl. Phys. **52**(12), 7182–7190 (1981).

[72] R. W. Hockney, S. Goel, and J. Eastwood, "Quiet high-resolution computer models of a plasma," J. Comput. Phys. **14**(2), 148–158 (1974).

[73] C. P Lamas, C. Vega, E. G Noya, and E. Sanz, "The water cavitation line as predicted by the TIP4P/2005 model," J. Chem. Phys. **158**(12), 124504 (2023).

[74] T. Darden, D. York, and L. Pedersen, "The effect of long-range electrostatic interactions in simulations of macromolecular crystals: A comparison of the Ewald and truncated list methods," J. Chem. Phys. **99**(10), 10089 (1993).

[75] U. Essmann, L. Perera, M. L. Berkowitz, T. Darden, H. Lee, and L. G. Pedersen, "A smooth particle mesh Ewald method," J. Chem. Phys. **103**(19), 8577–8593 (1995).

25 August 2025 10:07:37

[76] B. Hess, H. Bekker, H. J. Berendsen, and J. G. Fraaije, "LINCS: A linear constraint solver for molecular simulations," J. Comput. Chem. **18**(12), 1463–1472 (1997).

[77] V. G. Baidakov, S. P. Protsenko, and A. O. Tipeev, "Surface free energy of the crystal–liquid interface on the metastable extension of the melting curve," JETP Lett. **98**, 801–804 (2014).

[78] F. Hrahsheh, I. Jum'h, and G. Wilemski, "Second inflection point of supercooled water surface tension induced by hydrogen bonds: A molecular-dynamics study," J. Chem. Phys. **160**(11), 114504 (2024).

[79] C. Vega and E. de Miguel, "Surface tension of the most popular models of water by using the test-area simulation method," J. Chem. Phys. **126**(15), 154707 (2007).

[80] X. Wang, K. Binder, C. Chen, T. Koop, U. Pöschl, H. Su, and Y. Cheng, "Second inflection point of water surface tension in the deeply supercooled regime revealed by entropy anomaly and surface structure using molecular dynamics simulations," Phys. Chem. Chem. Phys. **21**(6), 3360–3369 (2019).

[81] A. Gorfer, C. Dellago, and M. Sega, "High-density liquid (HDL) adsorption at the supercooled water/vapor interface and its possible relation to the second surface tension inflection point," J. Chem. Phys. **158**(5), 054503 (2023).

[82] D. Frenkel, "Simulations: The dark side," Eur. Phys. J. Plus **128**, 10–21 (2013).

[83] P. Montero de Hijes, J. R Espinosa, C. Vega, and C. Dellago, "Minimum in the pressure dependence of the interfacial free energy between ice Ih and water," J. Chem. Phys. **158**(12), 124503 (2023).

[84] X.-M. Bai and M. Li, "Calculation of solid–liquid interfacial free energy: A classical nucleation theory based approach," J. Chem. Phys. **124**(12), 124707 (2006).

[85] A. S. Skapski, "A theory of surface tension of solids—I application to metals," Acta Metall. **4**(6), 576–582 (1956).

[86] S. Lippmann, C. Simon, S. Zechel, M. Seyring, U. Schubert, G. Wilde, and M. Rettenmayr, "Determining solid/liquid interfacial energies in Al–Cu by curvature controlled melting point depression," Acta Mater. **147**, 113–121 (2018).

[87] M. Gündüz and J. Hunt, "The measurement of solid–liquid surface energies in the Al–Cu, Al–Si and Pb–Sn systems," Acta Metall. **33**(9), 1651–1672 (1985).

[88] S. Wilson, K. Gunawardana, and M. Mendelev, "Solid–liquid interface free energies of pure bcc metals and B2 phases," J. Chem. Phys. **142**(13), 134705 (2015).